LARGE EDDY SIMULATION OF BLUFF BODY STABILISED PREMIXED FLAMES USING FLAMELETS

James C. Massey*, Ivan Langella* and Nedunchezhian Swaminathan*
jcm97@cam.ac.uk
*Department of Engineering, University of Cambridge, Trumpington Street,
Cambridge CB2 1PZ, United Kingdom

Abstract

Large Eddy Simulations of an unconfined turbulent lean practical flame stabilised behind a bluff body burner are computed using structured and unstructured numerical solvers. Unstrained flamelets are used as the sub-grid scale combustion closure using constant and dynamic formulations to model the flame curvature parameter β_c. The model uses a presumed probability density function to calculate the filtered reaction rate. The aim of this study is to determine the numerical set-up that provides the most reliable results for the flame that is furthest from blow-off conditions (A1). This work will lead to modelling the flame closest to blow-off (A4) and the flame at blow-off conditions, since these flames are highly unstable. Comparisons will be drawn with experimental data obtained using PIV, OH chemiluminescence and OH-PLIF techniques.

Introduction

Bluff body burners with high reactant flow rates are often used in practical combustion systems, which include gas turbines, industrial burners, afterburners and ramjets. The flame is stabilised by an anchoring mechanism provided by the recirculation zone behind the bluff body. The recirculation zone provides a continuous supply of heat to ignite the incoming reactant mixture. However, achieving flame stabilisation for high-velocity flows is difficult and becomes more complex through the use of lean fuel-air mixtures. Stringent emission legislations today mean that more combustion system are moving towards operating under lean conditions, as they provide efficiency and environmental benefits. These include increased fuel economy and lower operating temperatures, which lead to reduction in NO_x, SO_x, particulate matter, CO and hydrocarbon emission levels. Lean combustion is prone to combustion instabilities which can lead to the occurrence of flame blow-off, which is treated here as the complete extinction of the flame. Flame blow-off is detrimental to combustion systems and should be avoided. However, the exact mechanism of blow-off in turbulent premixed flames is still not fully understood [1] and a good understanding of the turbulence-flame interactions of stable flames close to blow-off conditions is first required.

Practical combustors operate under turbulent conditions and this makes simulating this combustion computationally expensive, as it is difficult to capture the turbulence-chemistry interactions. Large Eddy Simulation (LES) has emerged as a powerful computational modelling tool due to its potential to capture unsteady phenomena, such as ignition and blow-off. For LES modelling, the larger scales are obtained by fully resolving the flow field down to a cut-off scale, based on a filter width Δ, and the remaining sub-grid scales (SGS) are modelled. The SGS closure models need to be chosen carefully since the reaction zone thickness of a premixed flame is expected to be lower than Δ for the LES and hence the majority of the combustion related processes occurs within the sub-grid scales. The main challenge with turbulent premixed combustion research is to accurately capture the interactions between turbulence and

the effects of chemistry in combustion. Various models for LES have been proposed to model the filtered reaction rate $\overline{\dot{\omega}}$, where some are built on algebraic expressions whilst others require additional transport equations. Reviews for turbulent reaction rate modelling for LES have been covered in [2–6] and these have been separated into flamelet and non-flamelet based models. Flamelet-based models are further subdivided into geometric and statistical models, where statistical based models included presumed Probability Density Function (PDF) approaches, which are considered here. The flamelet assumption treats the reaction zones as a series of thin one-dimensional structures, which makes LES a more practical tool because computational requirements are significantly reduced. These structures remain unperturbed by turbulent eddies and it is assumed that the combustion chemistry occurs within these flamelets.

The scope of this work is to investigate whether a flamelet based model can accurately capture the stabilisation of flames further away and close to blow-off conditions; this paper deals with the former case. The paper is organised as follows. An overview of the LES model, SGS closures, the experimental case to be studied and its corresponding computational model and boundary conditions will be explained. A discussion of the results from the computations will follow this and the final section will summarise the key findings from this work.

Numerical Modelling

Governing Equations for LES

The instantaneous balance equations for mass, momentum, reaction progress variable and total enthalpy are Favre-filtered to obtain the filtered transport equations for LES and are thus presented below Continuity:

$$\frac{\partial \overline{\rho}}{\partial t} + \frac{\partial \overline{\rho}\widetilde{U}_j}{\partial x_j} = 0 \tag{1}$$

Momentum:

$$\overline{\rho}\frac{\mathrm{D}\widetilde{U}_i}{\mathrm{D}t} = -\frac{\partial \overline{p}}{\partial x_i} + \frac{\partial}{\partial x_j}\left(\overline{\rho\nu}\left[\frac{\partial \widetilde{U}_i}{\partial x_j} + \frac{\partial \widetilde{U}_j}{\partial x_i}\right]\right) - \frac{\partial}{\partial x_j}\left(\overline{\rho U_j U_i} - \overline{\rho}\widetilde{U}_j\widetilde{U}_i\right) \tag{2}$$

Reaction progress variable:

$$\overline{\rho}\frac{\mathrm{D}\widetilde{c}}{\mathrm{D}t} = \overline{\dot{\omega}} + \frac{\partial}{\partial x_j}\left(\left[\overline{\rho\mathscr{D}} + \overline{\rho}\frac{\nu_T}{\mathrm{Sc}_T}\right]\frac{\partial \widetilde{c}}{\partial x_j}\right) \tag{3}$$

Total enthalpy:

$$\overline{\rho}\frac{\mathrm{D}\widetilde{h}}{\mathrm{D}t} = \frac{\partial}{\partial x_j}\left(\left[\overline{\rho\alpha} + \overline{\rho}\frac{\nu_T}{\mathrm{Sc}_T}\right]\frac{\partial \widetilde{h}}{\partial x_j}\right) \tag{4}$$

The final term in Eq. (2) represent the SGS stresses. The constant Smagorinsky model [7], the revised approach by Vreman [8] and a dynamic approach [9, 10] are used here to model the SGS stresses. Gradient hypotheses are used for the scalar flux terms and the turbulent Schmidt number is a constant value of $\mathrm{Sc}_T = 0.7$, if not solved dynamically. The final term that requires closure is the filtered mass-based reaction rate $\overline{\dot{\omega}}$ and is described next.

Combustion Closure

Flamelets are viewed as locally thin laminar flames, which remain unperturbed by turbulent eddies, and are distributed in space and time yielding a thicker and diffusive flame brush. There have been three methods proposed for using PDF-based methodologies for flamelet modelling

in LES. One of these uses an algebraic approach [11], whilst the strained flamelet and unstrained flamelet models use a presumed PDF along with transport equation to solve for the SGS variance of the progress variable $\sigma^2_{c,\mathrm{sgs}}$. It was demonstrated that the unstrained flamelet closure provided superior results compared to the algebraic and strained flamelets approaches [11, 12]. The unstrained flamelet approach has performed well under multi-regime turbulent premixed combustion in a bluff body burner [13].

The unstrained flamelet model uses a reaction progress variable c to describe how burnt a fuel-air mixture is, where values of zero and unity represent reactant and fully burnt conditions respectively. The unstrained flamelet closure for filtered reaction rate $\overline{\dot{\omega}}$ is therefore written as [14]

$$\overline{\dot{\omega}} = \int_0^1 \dot{\omega}(\zeta) P\left(\zeta;\widetilde{c},\sigma^2_{c,\mathrm{sgs}}\right) \mathrm{d}\zeta = \overline{\rho} \int_0^1 \frac{\dot{\omega}(\zeta)}{\rho} \widetilde{P}\left(\zeta;\widetilde{c},\sigma^2_{c,\mathrm{sgs}}\right) \mathrm{d}\zeta \tag{5}$$

where $\widetilde{P}\left(\zeta;\widetilde{c},\sigma^2_{c,\mathrm{sgs}}\right)$ is the density weighted PDF of c, ζ represents the sample space variable for c and the flamelet reaction rate and mixture density are denoted using $\dot{\omega}(\zeta)$ and ρ respectively. The shape of the SGS PDF is assigned using a Beta function for given values of c and $\sigma^2_{c,\mathrm{sgs}}$, which are obtained from their respective transport equations. Equation (3) is used to obtain $\widetilde{c}$ whilst its corresponding variance is obtained by the following transport equation

$$\overline{\rho}\frac{\mathrm{D}\sigma^2_{c,\mathrm{sgs}}}{\mathrm{D}t} = \frac{\partial}{\partial x_j}\left(\left[\overline{\rho\mathscr{D}} + \overline{\rho}\frac{\nu_T}{\mathrm{Sc}_T}\right]\frac{\partial \sigma^2_{c,\mathrm{sgs}}}{\partial x_j}\right) + 2\left(\overline{\dot{\omega}c} - \overline{\dot{\omega}}\widetilde{c}\right) - 2\overline{\rho}\widetilde{\varepsilon}_c + 2\overline{\rho}\frac{\nu_T}{\mathrm{Sc}_T}\left(\frac{\partial \widetilde{c}}{\partial x_j}\frac{\partial \widetilde{c}}{\partial x_j}\right) \tag{6}$$

Only the third and fourth terms in Eq. (6) require closure. The first part of the reaction source term is closed as

$$\overline{\dot{\omega}c} = \overline{\rho}\int_0^1 \left(\frac{\dot{\omega}\zeta}{\rho}\right)\widetilde{P}(\zeta)\,\mathrm{d}\zeta \tag{7}$$

The fourth term represents the sub-grid dissipation rate of c. It is modelled using an algebraic closure [15], which has been successfully applied for the unstrained flamelet model [12, 13, 16]. The expression is given as

$$\widetilde{\varepsilon}_c = \left[1 - \exp\left(-\theta_5\Delta^+\right)\right] \times \left[2K_c\frac{s_L}{\delta_{\mathrm{th}}} + (C_3 - \mathscr{T}C_4\mathrm{Da}_\Delta)\left(\frac{2u'_\Delta}{3\Delta}\right)\right]\frac{\sigma^2_{c,\mathrm{sgs}}}{\beta_c}, \tag{8}$$

with $\theta_5 = 0.75$ being a constant and the LES filter width is normalised according to $\Delta^+ = \Delta/\delta_{\mathrm{th}}$. The unstrained flame thickness δ_{th} is calculated beforehand, along with its planar laminar flame speed s_L and the heat release parameter $\mathscr{T} = \rho_R/\overline{\rho} - 1$.

The SGS Damköhler number is $\mathrm{Da}_\Delta = \tau_{\mathrm{sgs}}/\tau_C$, which is the ratio of the SGS time scale $\tau_{\mathrm{sgs}} = k_{\mathrm{sgs}}/\varepsilon_{\mathrm{sgs}}$ to the chemical timescale $\tau_C = \delta_{\mathrm{th}}/s_L$. The SGS time scale can be related to the ratio of the SGS velocity scale u'_Δ, which needs to be modelled, and the filter width Δ so that $\tau_{\mathrm{sgs}} = \Delta/u'_\Delta$. Therefore the Damköhler number can be written in terms of normalised quantities $\mathrm{Da}_\Delta = \Delta^+/u'^+_\Delta$, with $u'^+_\Delta = u'_\Delta/s_L$ [15]. The remaining parameters signify influences of thermochemical and turbulence processes. The thermochemical parameter K_C is approximated as $K_C = 0.79\mathscr{T}$ [12]. The other constants $C_3 = 1.5\sqrt{\mathrm{Ka}_\Delta}/(1+\sqrt{\mathrm{Ka}_\Delta})$ and $C_4 = 1.1/(1+\mathrm{Ka}_\Delta)^{0.4}$ are both functions of the parameter Ka_Δ, calculated as $\mathrm{Ka}_\Delta = \sqrt{u'^{+3}_\Delta/\Delta^+}$ [15]. The SGS velocity scale u'_Δ is to be modelled. The scale-similarity approach has proved to be successful in

earlier studies [12, 16] and is given as [17]

$$u'_\Delta = C_q \sum_j |\widetilde{U}_j - \widehat{\widetilde{U}}_j|, \tag{9}$$

where $C_q = 1$ if a Gaussian test-filter in conjunction with an implicit Gaussian LES filter, and $\widehat{\widetilde{U}}_j$ represents the test-filtered velocity field. The final term that needs closure is the parameter β_c, where the term $\sigma^2_{c,\mathrm{sgs}}/\beta_c$ describes the flame curvature influenced by wrinkling. This can be solved by using a constant value or using a dynamic procedure based on the scale similarity approach [16]. The test filter for the dynamic procedure is $\widehat{\Delta} \approx 2\Delta$, with the filter width estimated as $\Delta = \mathscr{V}^{1/3}$, where $\mathscr{V}$ denotes the volume of a grid cell.

The Favre-filtered temperature can be directly obtained from the enthalpy according to $\widetilde{T} = T_0 + (\widetilde{h} - \widetilde{\Delta h}^0_f)/\widetilde{c}_p$, where $\widetilde{\Delta h}^0_f$ and $\widetilde{c}_p$ represent the formation enthalpy and specific heat capacity at constant pressure of the gas mixture and at a reference temperature $T_0 = 298.15\,\mathrm{K}$. The mixture density is computed as $\overline{\rho} = \overline{p}\widetilde{M}/\Re^0\widetilde{T}$, where $\widetilde{M}$ represents the Favre-filtered mixture molecular weight and $\Re^0$ is the universal gas constant.

Burner and Flame Conditions

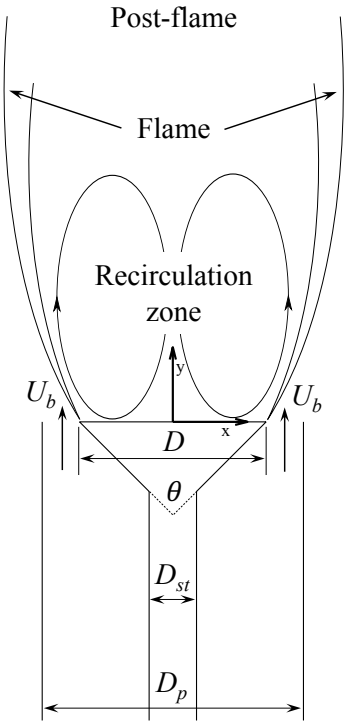

Figure 1: Schematic of the burner.

Flame	U_b (m/s)	ϕ
A1	21.6	0.75
A2	21.5	0.70
A3	21.4	0.67
A4	21.4	0.64

Table 1: Conditions for the burner.

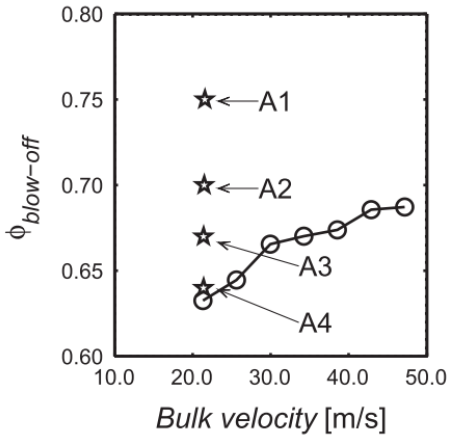

Figure 2: Blow-off curve [18, 19].

The burner to be studied here was developed by Balachandran et al. [18] and experimental data has been obtained in [19, 20], which will be used to validate the computations performed here. This burner has been recently studied from a computational perspective in [21–23]. A conical bluff body with diameter $D = 25\,\mathrm{mm}$ and apex angle $\theta = 90^\circ$ was mounted to a circular rod with a stem diameter $D_{st} = 6.35\,\mathrm{mm}$. The bluff body was fitted within a concentric pipe with diameter $D_p = 35\,\mathrm{mm}$ and the bluff body base was exposed to open air at atmospheric conditions, as illustrated in Fig. 1. Methane and air at ambient conditions were premixed and

entered the annular section at a constant mass flow rate in order to provide the required bulk velocity U_b at the bluff body base. The burner was run at four conditions, displayed in Table 1 where the fuel-air equivalence ratio was decreased starting from far away from blow-off (A1) to just prior to blow-off (A4), as shown in Fig. 2. Experimental measurements were obtained using PIV, OH* chemilluminescence and OH-PLIF techniques, as described in [19].

Computational Solver and Grid

Two numerical solvers will be used for this case, namely PRECISE-MB and PRECISE-UNS and these codes are used for structured and unstructured grids respectively. PRECISE-UNS inherited part of the combustion modelling framework from the structured code PRECISE-MB [24] and uses the numerical infrastructure based on DOLFYN for unstructured grids. The gradients are calculated through the use of second-order accurate central difference schemes [25]. A constant time step is specified in order to satisfy the Courant-Friedrichs-Lewy (CFL) condition by ensuring the CFL number does not exceed 0.3.

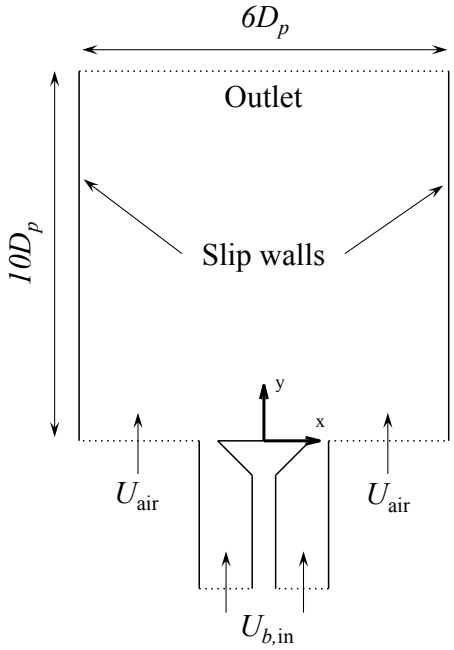

Figure 3: Computational grid and boundary conditions for the burner (not to scale).

Parameter	Value
D	25 mm
D_p	35 mm
D_{st}	6.35 mm
T	298 K
U_{air}	0.1 m/s
U_b	21.6 m/s
$U_{b,\text{in}}$	10.9 m/s
θ	90°

Table 2: Parameters for the LES of the bluff body burner [19].

The computational grid starts 70 mm upstream of the bluff body base and a region of $10D_p \times 6D_p \times 6D_p$ is added from the bluff body base as depicted in Fig. 3. The mesh for -MB had 3 million cells in total, using refinement at the bluff body and shear layers with a minimum cell size of 0.2 mm. The mesh for -UNS comprised of 4 million hexahedral cells with refinement towards the flame's location and the shear layers, where the minimum cell size was 0.3 mm. The operating parameters for the burner are shown in Table 2. A flat velocity profile at the pipe inlet with magnitude $U_{b,\text{in}}$ was specified with a value to give the required reference bulk velocity at the bluff body base. An additional velocity stream $U_{b,\text{air}}$ is included to mimic the ambient air entrainment around the bluff body. Slip wall conditions are included downstream of the bluff body to the outlet of the domain. The GRI 3.0 chemical mechanism was used to determine the properties for an unstrained laminar flamelet. The desired equivalence ratio is obtained by setting the correct mixture fraction ξ at the pipe inlet in order to obtain the chemical properties of the mixture, such as $\widetilde{\Delta h}^0_f$, $\widetilde{c}_p$ and $\widetilde{M}$ as functions of $\widetilde{c}$ and $\sigma^2_{c,\text{sgs}}$. The resolution

in the table for $\widetilde{c}$ and $\sigma^2_{c,\mathrm{sgs}}$ are 101 and 51 evenly distributed points from 0 to 1 respectively. The progress variable is based on the sum of the mass fractions for CO_2 and CO. The flame curvature parameter for Eq. (8) uses a value $\beta_c = 0.4$ when it is not modelled dynamically. The time-averaged statistics were taken across eight flow-through times, where the reference length was taken to be 100 mm.

Results and Discussion

Isothermal Flow Results

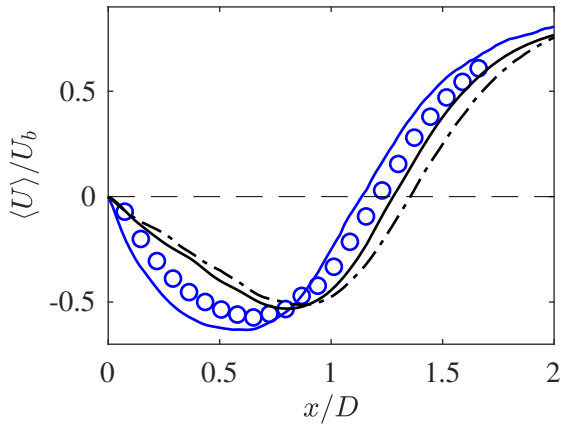

Figure 4: Variation of $\langle U \rangle / U_b$ for the isothermal LES calculations (lines) and measured data (○) [19] along the centreline. (——) represents the results from PRECISE-MB, and (–·–) and (——) represent the results from PRECISE-UNS using the constant Smagorinsky model and and revised Vreman approach.

An isothermal flow simulation was performed first to validate the numerical set-up and the flow field, in order to ensure that the correct turbulence model was used. The simulations were compared against the velocity PIV measurements obtained in [19]. It was necessary to initially validate the length of the recirculation zone and the results are depicted in Fig. 4. The two curves from -UNS compare the two constant Smagorinsky approaches, where the recirculation zone lengths were $1.35D$ and $1.27D$ for the constant Smagorinsky model and Vreman model respectively. The approach by Vreman gave superior results because the recirculation zone

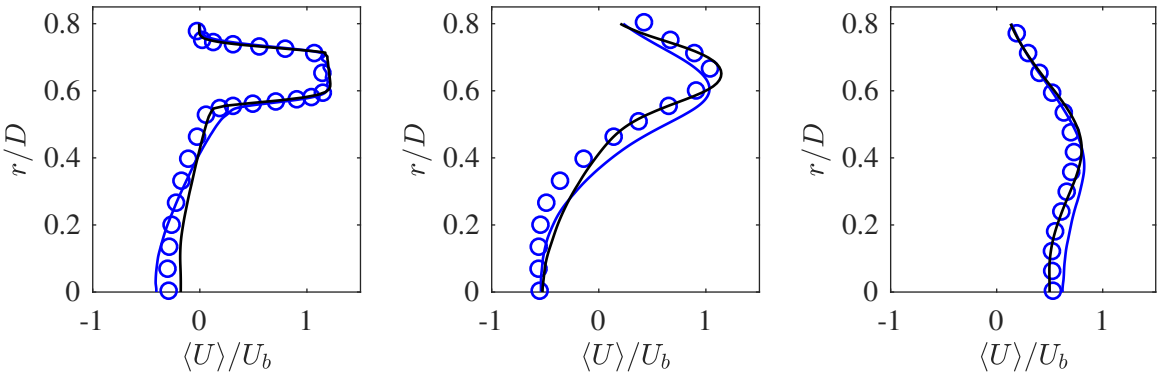

(a) $x/D = 0.2$ **(b)** $x/D = 0.8$ **(c)** $x/D = 1.6$

Figure 5: Radial variations of $\langle U \rangle / U_b$ using the same legend as in Fig. 4.

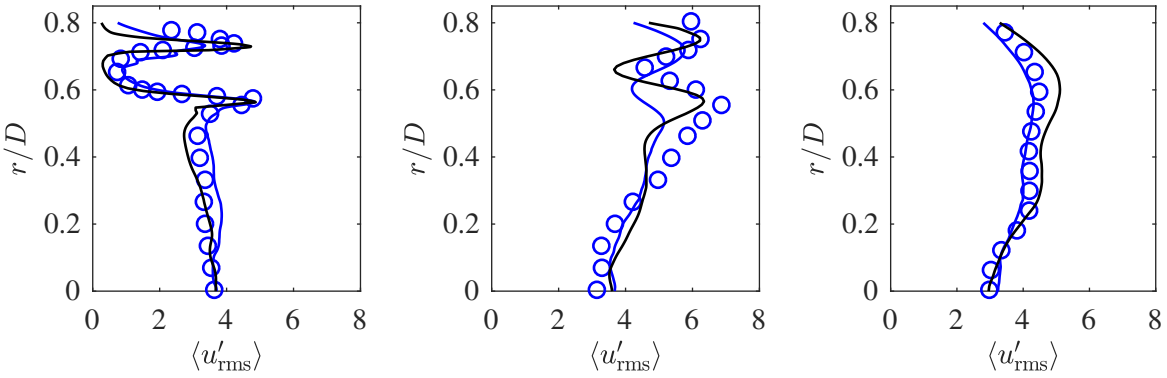

(a) $x/D = 0.2$ **(b)** $x/D = 0.8$ **(c)** $x/D = 1.6$

Figure 6: Radial variations of $\langle u'_{\mathrm{rms}} \rangle$ using the same legend as in Fig. 4.

length was closer to the experimentally observed value of $1.21D$. In addition the positive velocity gradients were captured more accurately with this approach. This would support the view that the Vreman approach gives improved results for turbulent flows in engineering applications [8]. The calculation performed using -MB produced a recirculation zone length of $1.13D$, although velocity profile in the recirculation zone was captured better than those from -UNS. The -MB run used the dynamic Smagorinsky resulted in the expected improvements. The dynamic approach for UNS is under development.

Some further analysis of the recirculation zone is conducted by studying the radial variations of axial velocity and its root-mean-square (rms) values, illustrated in Figs. 5 and 6. These streamwise locations were close to the bluff body base (a), within the wider region of the recirculation zone (b) and downstream of the recirculation zone (c). It was chosen to omit the constant Smagorinsky approach for analysis, due to the improved results produced by the Vreman model. Both simulations captured the axial velocity profiles well and this was also the case for the axial rms velocity profiles. The calculation using -MB underpredicted the rms velocity, as in Fig. 6b.

Reacting Flow Results

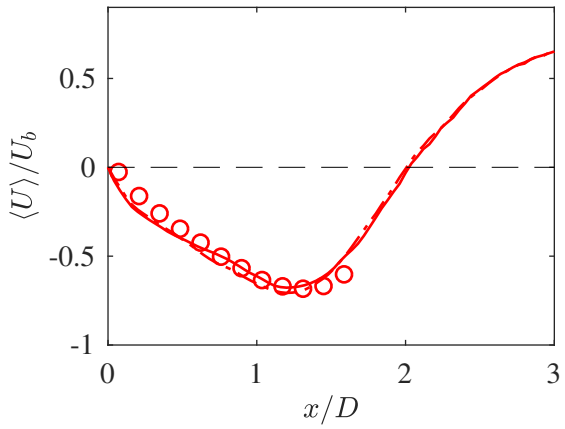

Figure 7: Variation of $\langle U \rangle / U_b$ for the reacting computations performed using PRECISE-MB (lines) and measured data (○) [19] along the centreline. (——) and (–·–) represent constant and dynamic β_c approaches respectively.

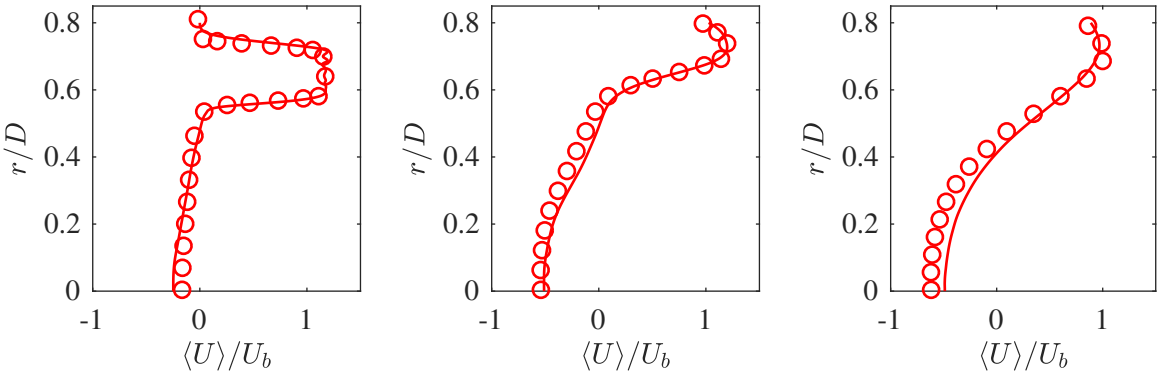

(a) $x/D = 0.2$ **(b)** $x/D = 0.8$ **(c)** $x/D = 1.6$

Figure 8: Radial variations of $\langle U \rangle / U_b$ using the same legend as in Fig. 7.

The flame chosen to be computed here was flame A1, which was the flame furthest from blow-off conditions, as illustrated in Fig. 2. This was to determine which of the turbulence SGS closure and code could capture the flame's flow field the best since there was little to differentiate between the results for the isothermal calculation. The work for the computation using -UNS is still ongoing due to the higher computational costs and thus only results are shown from -MB from this point onwards. The centreline axial velocity variation is shown in Fig. 7, where the two computations compared static and dynamic modelling approaches for β_c in Eq. (8) for $\widetilde{\varepsilon}_c$. The value $\beta_c = 0.4$ for the static case closely matched the results from the dynamic formulation and thus it was decided to bound the dynamic formulation for a minimum value of $\beta_c = 0.4$ to ensure that the scalar dissipation rate doesn't fall below zero and the flame remains fully turbulent. The radial variations for axial velocity at different locations are shown in Fig. 8, where the comparison is only made between the results from the computation using the dynamic approach with the previously mentioned modification for β_c. It can be seen that there is a very good agreement between experimental data and the computation. However, the recirculation zone here has to be estimated from the computations because data was not obtained for the whole of the recirculation zone. It is noted though that the recirculation zone length is sensitive to the effect of combustion since there was an increase in length from $1.13D$ to $2.02D$.

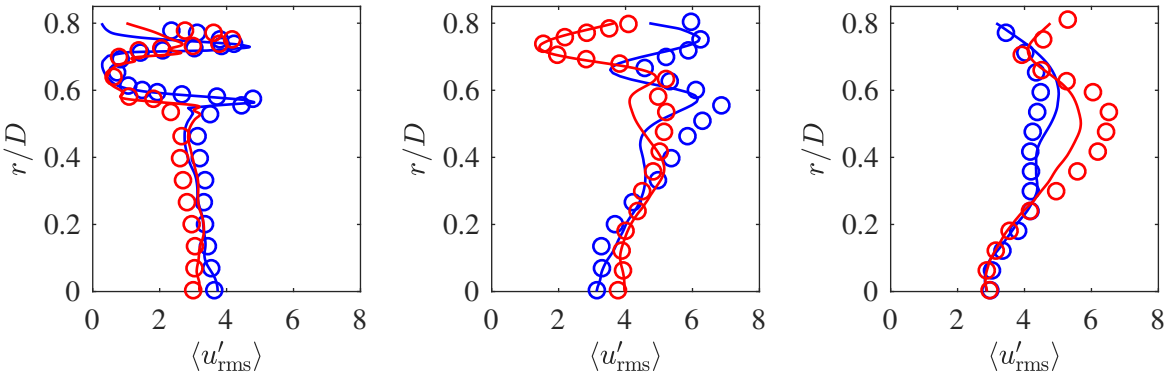

(a) $x/D = 0.2$ **(b)** $x/D = 0.8$ **(c)** $x/D = 1.6$

Figure 9: Radial variations of $\langle u'_{\text{rms}} \rangle$. Symbols denote the experimental data and lines represent the LES calculations. Blue and red represent isothermal and reacting conditions respectively.

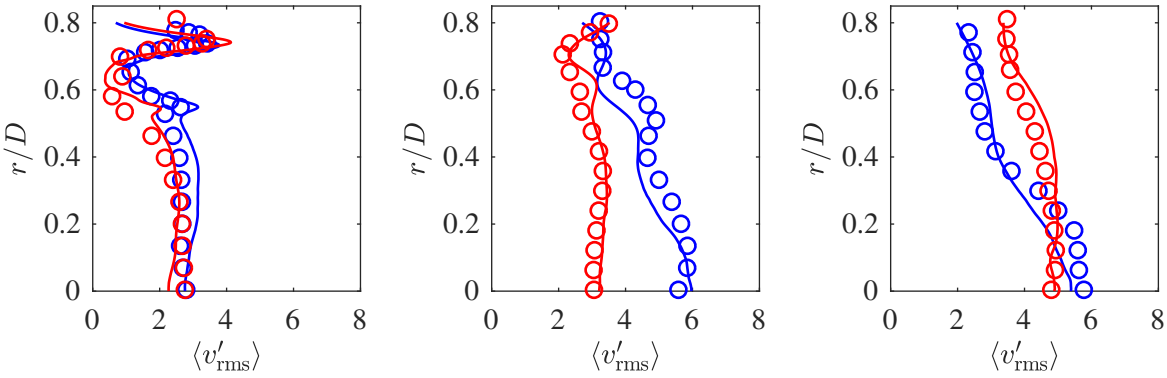

(a) $x/D = 0.2$ **(b)** $x/D = 0.8$ **(c)** $x/D = 1.6$

Figure 10: Radial variations of $\langle v'_{\mathrm{rms}} \rangle$ using the same legend as in Fig. 9.

The results for the axial and radial rms value variations for flame A1 are shown in Figs. 9 and 10 respectively and these are compared to the isothermal results. It was shown that the effect of combustion at $x/D = 0.2$ caused little difference to the turbulence levels since this location was close to the bluff body. The discrepancy between the results at $x/D = 0.8$ was caused by the difference in the structure of the recirculation zone since the sizes were different. The turbulence levels were higher for isothermal conditions at this location since the recirculation zone here was significantly smaller. The turbulence levels at $x/D = 1.6$ were different since this location was within the recirculation zone for reacting conditions and hence the turbulence levels increased downstream from the bluff body. The turbulence levels decreased at this location for the isothermal results since this location was beyond the recirculation zone.

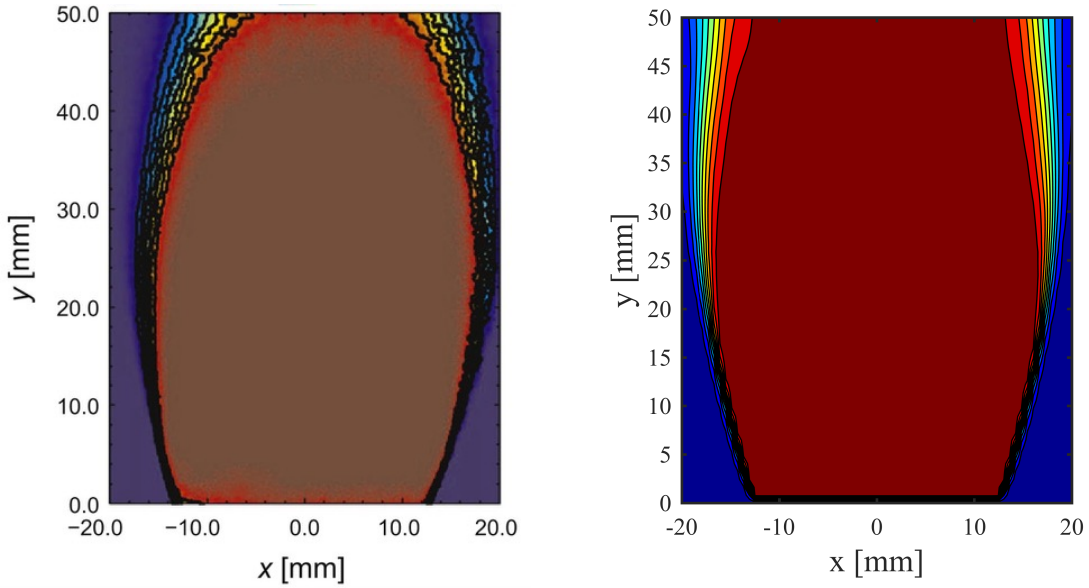

(a) OH-PLIF [19]. **(b)** LES

Figure 11: Comparison of the experimental flame photograph with the time-averaged reaction progress variable field from the LES for flame A1. Contours are at increments of $\widetilde{c} = 0.1$.

Some additional qualitative comparisons are made by the use of the OH-PLIF data collected in [19]. Fig. 11 shows the mean reaction progress variable field and Fig. 12 shows a comparison of normalised OH and normalised mean reaction rate from the experiment and LES respectively.

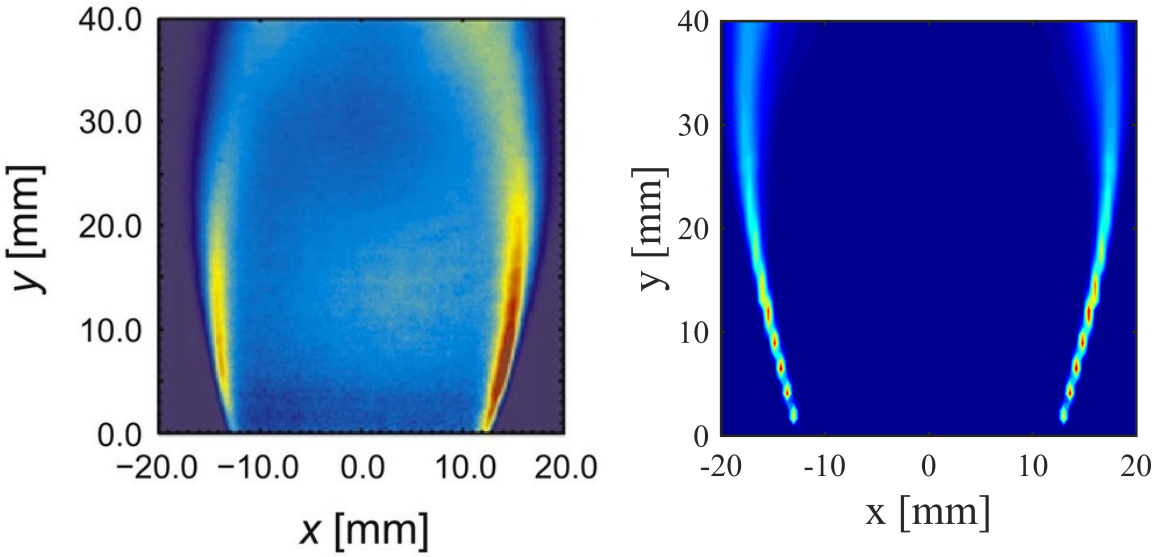

(a) OH-PLIF [19].

(b) Filtered reaction rate.

Figure 12: Comparison of the normalised OH-PLIF and normalised filtered reaction rate.

The flame thickness increases downstream from the bluff body base due to turbulent eddies perturbing the flame brush. This is also shown in Fig. 12 since the normalised quantities are highest in the region closest to the bluff body base. The contour spacing for Fig. 11 was larger at the furthest downstream point from the bluff body base examined, showing a thicker flame and consequently caused a lower reaction rate as shown in Fig. 12b. Nonetheless the contour spacing in Fig. 11 is still small, showing that the flame is stable. It can also be seen in Figs. 11 and 12 that the width between the flame brushes for the computations is higher from $y > 40\,\text{mm}$, suggesting the flame length is overpredicted in computation.

Conclusions and Suggested Further Work

Large Eddy Simulations using structured and unstructured CFD codes were undertaken to model a turbulent lean premixed bluff body stabilised flame. The flame furthest from blow-off conditions (A1) was modelled. The SGS closure performance was first evaluated using a non-reacting flow and it was found that the Vreman closure gave improved results for the cold flow compared to the dynamic Smagorinsky model. This relative evaluation for the reacting flow is on-going and will be discussed in the presentation. The combustion model involves a parameter, β_c, related to flamelet curvature/wrinkling, which can be evaluated dynamically. The reacting flow results obtained using -MB with dynamic Smagorinsky closure and both static and dynamic approaches for β_c are presented and discussed for the flame A1 as a first step towards predicting the flame blow-off behaviour. It was seen that the recirculation zone length was highly sensitive to combustion, since the levels of turbulence were low. In addition, it was seen in both isothermal and reacting calculations that the turbulence levels increased downstream of the bluff body base within the recirculation zone. The isothermal results also showed that the turbulence levels decreased downstream from the recirculation zone.

Acknowledgements

The author is grateful to EPSRC and Rolls-Royce plc. for their support.

Nomenclature

Roman

c	reaction progress variable
D	bluff body diameter
$\mathscr{D}$	molecular diffusivity
h	total enthalpy per unit mass
P	PDF
Sc_T	turbulent Schmidt number
s_L	laminar flame speed
$\mathscr{T}$	heat release parameter
U_b	reference bulk velocity
u'_Δ	sub-grid scale velocity

Greek

α	thermal diffusivity
β_c	flame curvature parameter
Δ	LES filter width
δ_{th}	unstrained laminar flame thickness
$\widetilde{\varepsilon}_c$	sub-grid scalar dissipation rate
ζ	sample space variable for c
ν_T	kinematic residual eddy-viscosity
ξ	mixture fraction
ρ	mixture density
$\sigma^2_{c,\mathrm{sgs}}$	sub-grid scale variance of c
ϕ	fuel-air equivalence ratio
$\dot{\omega}$	mass-based reaction rate

Superscripts

$+$	normalised quantity

Subscripts

Δ	sub-grid scale quantity
P	product (fully burnt) conditions
R	reactant (fully unburnt) conditions
sgs	sub-grid scale quantity
T	turbulent quantity

Operators

$\overline{\varphi}$	simple filtering of φ
$\widetilde{\varphi}$	Favre filtering of φ
$\widehat{\varphi}$	test filtering of φ
$\langle\varphi\rangle$	time-average of φ

References

[1] Shanbhogue, S.J., Husain, S., Lieuwen, T.C., "Lean blowoff of bluff body stabilized flames: Scaling and dynamics", *Prog. Energy Combust. Sci.* 35(1): 98–120 (2009).

[2] Pitsch, H., "Large-Eddy Simulation of Turbulent Combustion", *Annu. Rev. Fluid Mech.* 38(1): 453–482 (2006).

[3] Poinsot, T., Veynante, D., *Theoretical and Numerical Combustion*, 3rd ed. (2012).

[4] Cant, R.S., "RANS and LES Modelling of Premixed Turbulent Combustion", in *Turbul. Combust. Model. Adv. New Trends Perspect.*, edited by T. Echekki, E. Mastorakos, chap. 4,

pp. 63–90, Springer Netherlands (2011).
[5] Swaminathan, N., Bray, K.N.C., "Fundamentals and Challenges", in *Turbul. Premixed Flames*, edited by N. Swaminathan, K.N.C. Bray, chap. 1, pp. 1–40, Cambridge University Press (2011).
[6] Gicquel, L.Y.M., Staffelbach, G., Poinsot, T., "Large Eddy Simulations of gaseous flames in gas turbine combustion chambers", *Prog. Energy Combust. Sci.* 38(6): 782–817 (2012).
[7] Smagorinsky, J., "General circulation experiments with the primitive equations", *Mon. Weather Rev.* 91(3): 99–164 (1963).
[8] Vreman, A.W., "An eddy-viscosity subgrid-scale model for turbulent shear flow: Algebraic theory and applications", *Phys. Fluids* 16(10): 3670–3681 (2004).
[9] Germano, M., Piomelli, U., Moin, P., Cabot, W.H., "A dynamic subgrid-scale eddy viscosity model", *Phys. Fluids A Fluid Dyn.* 3(7): 1760–1765 (1991).
[10] Lilly, D.K., "A proposed modification of the Germano subgrid-scale closure method", *Phys. Fluids A Fluid Dyn.* 4(3): 633–635 (1992).
[11] Langella, I., *Large Eddy Simulation of Premixed Combustion*, Ph.D. thesis, University of Cambridge, UK (2015).
[12] Langella, I., Swaminathan, N., "Unstrained and strained flamelets for LES of premixed combustion", *Combust. Theory Model.* 20(3): 410–440 (2016).
[13] Langella, I., Swaminathan, N., Pitz, R.W., "Application of unstrained flamelet SGS closure for multi-regime premixed combustion", *Combust. Flame* 173: 161–178 (2016).
[14] Cook, A.W., Riley, J.J., "A subgrid model for equilibrium chemistry in turbulent flows", *Phys. Fluids* 6(8): 2868 (1994).
[15] Dunstan, T.D., Minamoto, Y., Chakraborty, N., Swaminathan, N., "Scalar dissipation rate modelling for large eddy simulation of turbulent premixed flames", *Proc. Combust. Inst.* 34(1): 1193–1201 (2013).
[16] Langella, I., Swaminathan, N., Gao, Y., Chakraborty, N., "Assessment of dynamic closure for premixed combustion large eddy simulation", *Combust. Theory Model.* 19(5): 628–656 (2015).
[17] Pope, S.B., *Turbulent Flows*, Cambridge University Press (2000).
[18] Balachandran, R., Ayoola, B.O., Kaminski, C.F., Dowling, A.P., Mastorakos, E., "Experimental investigation of the non linear response of turbulent premixed flames to imposed inlet velocity oscillations", *Combust. Flame* 143(1-2): 37–55 (2005).
[19] Kariuki, J., Dawson, J.R., Mastorakos, E., "Measurements in turbulent premixed bluff body flames close to blow-off", *Combust. Flame* 159(8): 2589–2607 (2012).
[20] Kariuki, J., *Turbulent premixed flame stabilization and blow-off*, Ph.D. thesis, University of Cambridge, UK (2013).
[21] Farrace, D., Chung, K., Pandurangi, S.S., Wright, Y.M., Boulouchos, K., Swaminathan, N., "Unstructured LES-CMC modelling of turbulent premixed bluff body flames close to blow-off", *Proc. Combust. Inst.* 36(2): 1977–1985 (2017).
[22] Hodzic, E., Alenius, E., Duwig, C., Szasz, R.S., Fuchs, L., "A Large Eddy Simulation Study of Bluff Body Flame Dynamics Approaching Blow-Off", *Combust. Sci. Technol.* 189(7): 1107–1137 (2017).
[23] Hodzic, E., Jangi, M., Szasz, R.Z., Bai, X.S., "Large eddy simulation of bluff body flames close to blow-off using an Eulerian stochastic field method", *Combust. Flame* 181: 1–15 (2017).
[24] Anand, M.S., Zhu, J., Connor, C., Razdan, M.K., "Combustor Flow Analysis Using an Advanced Finite-Volume Design System", *ASME 1999 Int. Gas Turbine Aeroengine Congr. Exhib.* 2: 1–10 (1999).
[25] Ferziger, J.H., Perić, M., *Computational Methods for Fluid Dynamics*, Springer Berlin Heidelberg, Berlin, Heidelberg (2002).